



Day-Ahead Operation of an Urban Energy System Considering Traffic Flows and Peak Shaving

Yan Peng¹, Junchao Ma¹, Chengyu Lu¹, Sheng Chen^{2*} and Lei Pei²

¹State Grid Zhejiang Electric Power Research Institute, Hangzhou, China, ²The College of Energy and Electrical Engineering, Hohai University, Nanjing, China

With the increasing penetration of new-type loads such as electric vehicles and hydrogen fuel vehicles in urban power grids, the peak-to-valley load difference increases sharply, and a multi-energy coordination model is desirable. This article proposes a day-ahead operation model of an urban energy system considering traffic flows and peak shaving, which can positively contribute to multi-energy complement and low-carbon emission. The proposed model minimizes the total cost of electricity and gas by optimizing the charging and discharging strategies of energy storage, in which the output of the wind turbine and energy management of the energy hub are adaptively adjusted. The urban energy system is represented by a second-order cone (SOC) energy flow model, and hence, the optimization problem is modeled as a mixed integer SOC programming (MISOCP). Finally, test results on an integrated urban energy network indicate that the energy storage and multi-energy coordination can alleviate the peak load cutting and valley filling. The relationship between urban grid operation cost and peak-valley difference is also discussed. The maximum utilization of renewable energy sources using gasoline vehicles has been presented in this study to illustrate cost and emission reductions for a sustainable integrated electricity and transportation infrastructure.

Keywords: an urban energy system, peak shaving, traffic flows, multi-energy complement, low-carbon operation

OPEN ACCESS

Edited by:

Qinran Hu,
Southeast University, China

Reviewed by:

Hossam A. Gabbar,
Ontario Tech University, Canada
Chuan He,
Sichuan University, China
Shuai Lu,
Southeast University, China

*Correspondence:

Sheng Chen
chenshenghu@163.com

Specialty section:

This article was submitted to Smart Grids, a section of the journal Frontiers in Energy Research

Received: 25 February 2022

Accepted: 28 March 2022

Published: 03 May 2022

Citation:

Peng Y, Ma J, Lu C, Chen S and Pei L (2022) Day-Ahead Operation of an Urban Energy System Considering Traffic Flows and Peak Shaving. *Front. Energy Res.* 10:883598. doi: 10.3389/fenrg.2022.883598

1 INTRODUCTION

1.1 Motivation

In recent years, energy consumption and global environmental problems have become increasingly serious, and the energy transition toward a low-carbon energy system is highly desirable (Zhao et al., 2017). The energy internet provides great potential for reliable power supply and an improved energy efficiency by integrating various energy production/conversion components, including renewable energy sources (RESs), energy storage systems (ESSs), hydrogen fuel vehicles (HVs), and electric vehicles (EVs) (Strasser et al., 2015; Meng and Wang, 2017; Yang and Fang, 2017). At the same time, interactions between urban electrical, transportation, and natural gas systems have become increasingly common due to the utilization of coupling components such as microturbines, combined heat and power (CHP), and power to gas units (Mancarella, 2014; Shabanpour-Haghighi and Seifi, 2015). The coupling of urban multi-energy networks positively contributes to the improved energy utilization efficiency, multi-energy complement, and the construction of a low-carbon sustainable energy system (Xu et al., 2020).

Traditionally, coupled energy systems have been operated and optimized independently (Chen et al., 2014). The urban distribution network that is inactive generally has limited ability to

regulate power flow, which results in the problem of a large difference between the daily peak and valley of the net load (Uddin et al., 2018). On the other hand, the traditional energy storage has relatively small storage capacity with a high investment cost, and hence, it is difficult to store energy effectively on a large scale and for a long time (Zhao et al., 2020). Considering the fact that the traditional urban distribution network cannot fully meet the electricity demand of new-type loads such as EVs and HVs, the development of day-ahead co-optimization of multi-energy systems is of considerable interest.

Owing to the aforementioned considerations, the present work develops a day-ahead co-optimization strategy for urban energy networks considering traffic flows.

1.2 Literature Review

1.2.1 Research on Power-Transportation Coordination

EVs and HVs have become a promising alternative to gasoline vehicles (GVs) for decarbonizing the transportation sector and combating climate change (IEA, Global EV Outlook, 2020). An integrated demand response framework is designed to regulate flexible resources in both networks through optimal road tolls and electricity tariffs in Lv et al., 2021a. In Rotering and Ilic (2011), the problem of growing peak load and grid overloading is addressed based on a forecast of future electricity prices, and the dynamic programming algorithm is employed to find the economically optimal solution for the vehicle owner. Hu et al. (2016) present an integrated optimization framework for battery sizing, charging, and on-road power management in plug-in hybrid EVs. The maximum utilization of RESs using GVVs has been presented in Saber and Venayagamoorthy (2011) to achieve cost and emission reductions, which contributes to a low-carbon integrated electricity and transportation infrastructure. We note that most works consider the coupling between the transportation system and the power grid. However, the coupling between the power, natural gas, and the transportation system has not been well considered.

1.2.2 Coordinated Optimization of Multi-Energy Systems

A day-ahead optimal scheduling of the urban energy system is proposed by Jin et al., 2016, in which the flexible and reconfigurable topology of power distribution networks is considered. The joint and unified optimization decision of coupled power systems and natural gas systems is analyzed in Martínez-Mares et al. (2011). Correa-Posada and Sánchez-Martín (2015) determine the dynamic optimal operation strategy of the electricity-gas integrated energy system, which includes a transient natural-gas flow model. An integrated electricity-gas system with steady-state energy flow models considering the uncertainty of wind power is proposed in Gao and Li (2020). Additionally, a new Benders decomposition-based algorithm is proposed, which improves the solution efficiency for non-convex models (Gao and Li, 2021). A new external dependency model based on the energy hub (EH) is introduced to consider the possible uncertainty in customer decision through stochastic

model processing (Neyestani et al., 2015). The stochastic optimal model is investigated with the comprehensive consideration of renewable generation and carbon-capture-based power-to-gas technology (Li et al., 2018). However, we note that most existing works on coordination optimization of integrated energy systems do not consider the existence of new-type loads such as EVs and HVs. Moreover, in most existing studies, a common assumption is that the driving mode of EVs is known. Arrival rates and times as well as the number of charging requests are specified in advance in a deterministic or stochastic manner, which can be determined from data-driven methods or queuing theory or modeled with probabilistic models through Markov decision processes. This assumption is reasonable for set-level research, such as residential parking management or a single CS management. However, it may not be appropriate if the system-level interdependency is under investigation, which is proposed in this article.

1.3 Contribution of This Study

To fill the research gaps summarized above, our model makes the following contributions:

- 1) We propose a mixed-UE traffic flow model based on an urban transportation system and divide the overall vehicular flows into five categories: GV traffic flow, EV traffic flow, HV traffic flow, HV charging flow, and EV charging flow. Our model, hence, accurately simulates the distribution of EVs and HVs in the urban transportation network.
- 2) We develop a day-ahead optimal dispatch of an urban energy system considering the transportation-network operation model, which includes the electric-gas co-optimization and the impact of traffic flows. Our model positively contributes to multi-energy complement and low-carbon operation. Moreover, the optimal energy management of EHs reduces the peak-valley difference caused by increasing penetrations of new-type loads such as EVs and HVs.

The remainder of this article is organized as follows: **Section 2** elaborates on the mathematical model of day-ahead operation for an urban energy system considering traffic flows. **Section 3** presents the performance of the proposed optimization model. Finally, **Section 4** presents the conclusions of the work.

2 DAY-AHEAD OPERATION OF AN URBAN ENERGY SYSTEM CONSIDERING PEAK LOAD SHAVING

This section first presents the day-ahead electricity-gas co-optimization for urban energy systems, which includes the operating constraint with regard to peak load shaving. Then, the joint optimal dispatch model considers the electricity charging load and hydrogen charging load on the traffic side. Finally, through the optimal control of ESS and energy management of EH, the peak shaving and valley filling of the urban system with

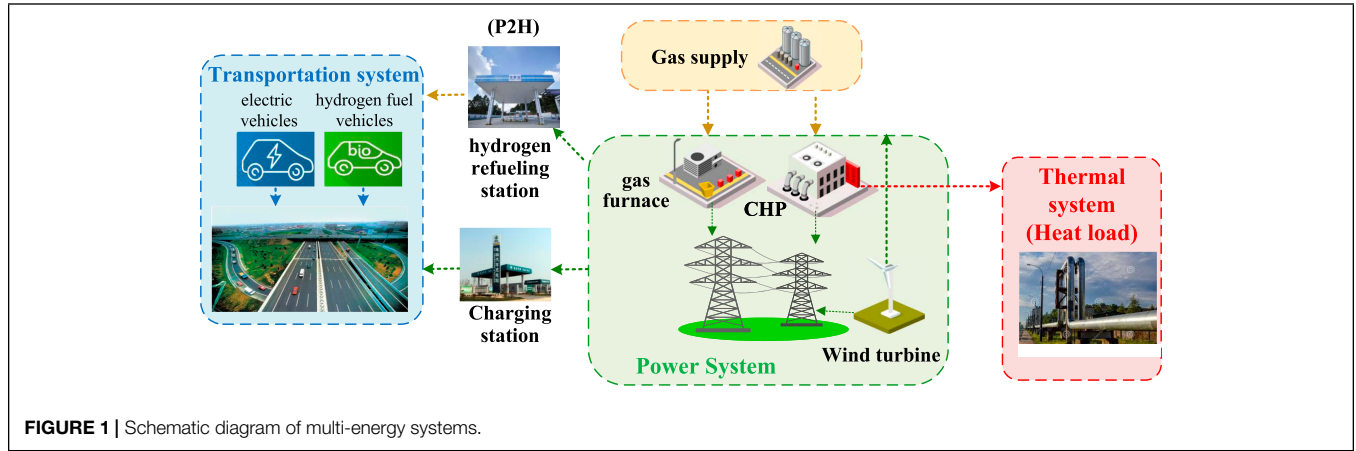


FIGURE 1 | Schematic diagram of multi-energy systems.

high penetrations of wind power are realized. The multi-energy systems are shown in **Figure 1**. There are many nodes connected to EH in the urban distribution network. EH provides hydrogen for the hydrogen charging station on the traffic side through the internal P2H device, meets the heat load demand through the CHP unit, and provides power for the charging station on the traffic side simultaneously through the converter and CHP unit.

Five key assumptions are made in our work:

- 1) We use a nonlinear day-ahead optimal dispatch model of an urban energy system that considers the transportation-network operation model.
- 2) We use fixed natural gas price information to coordinate the operation of electricity and natural gas systems. Unfixed gas pricing often leads to market inefficiencies.
- 3) We assume that the wind power output is deterministic, without considering the randomness of wind power output.
- 4) We use time-of-use price to calculate the cost of purchasing electricity in an urban energy system.

2.1 Branch Flow Model of the Urban Power Distribution Network

Since AC power flow constraints are non-convex, the day-ahead dispatch of the urban energy system is a non-convex optimization problem, which is difficult to solve. The second-order cone (SOC) relaxation based on the branch flow model is implemented to improve its computational tractability. Therefore, we use the branch flow model to replace the nonlinear power flow model of the urban distribution network (Baran and Wu, 1989):

$$\tilde{U}_{i,t} = U_{i,t}^2, \forall i \in \Omega^{node}, \forall t \in T, \quad (1)$$

$$\tilde{I}_{ij,t} = I_{ij,t}^2, \forall ij \in \Omega^{line}, \forall t \in T, \quad (2)$$

$$\begin{cases} \sum_{j \in M(i)} P_{ij,t} - \sum_{k \in N(i)} (P_{ki,t} - \tilde{I}_{ki,t} R_{ki,t}) = P_{i,t}^{inj} \\ \sum_{j \in M(i)} Q_{ij,t} - \sum_{k \in N(i)} (Q_{ki,t} - \tilde{I}_{ki,t} X_{ki,t}) = Q_{i,t}^{inj} \end{cases} \forall i \in \Omega^{node}, \forall t \in T, \quad (3)$$

$$\tilde{U}_{j,t} = \tilde{U}_{i,t} - 2(P_{ij,t} R_{ij,t} + Q_{ij,t} X_{ij,t}) + \tilde{I}_{ij,t} (R_{ij}^2 + X_{ij}^2) \forall ij \in \Omega^{node} \forall ij \in \Omega^{line}, \forall t \in T \quad (4)$$

$$\tilde{I}_{ij,t} \tilde{U}_{i,t} = P_{ij,t}^2 + Q_{ij,t}^2 \forall i \in \Omega^{node} \forall ij \in \Omega^{line}, \forall t \in T, \quad (5)$$

$$P_{i,t}^{inj} = P_{i,t}^{sub} + P_{i,t}^{DG} - P_{i,t}^L + P_{i,t}^{dis} - P_{i,t}^{ch} - P_{i,t}^{EH} - P_{i,t}^{GF} - P_{i,t}^{CHP} - P_{i,t}^{P2H}, \quad \forall i \in \Omega^{node}, \forall t \in T, \quad (6)$$

$$Q_{i,t}^{inj} = Q_{i,t}^{sub} + Q_{i,t}^{DG} - Q_{i,t}^L \forall i \in \Omega^{node}, \forall t \in T. \quad (7)$$

Eqs 1, 2 replace the voltage and current quadratic terms in the original nonlinear power flow equation with new variables. The DistFlow model for radial electricity networks is formulated by 3–7, in which variables of the squared voltage magnitude and squared branch current are employed. **Eqs 3–5** represent the active and reactive power flow balance. **Eqs 6, 7** represent the injected active and reactive power of the node.

The operation of the urban AC distribution network should satisfy the following security constraints:

$$\begin{cases} P_{i,t}^{sub} \leq P_{i,t}^{sub} \leq P_{i,t}^{sub\max} \\ Q_{i,t}^{sub} \leq Q_{i,t}^{sub} \leq Q_{i,t}^{sub\max} \end{cases} \forall i \in \Omega^{sub}, \forall t \in T, \quad (8)$$

$$P_{ij,t}^2 + Q_{ij,t}^2 \leq S_{ij\max}^2 \forall ij \in \Omega^{line}, \forall t \in T, \quad (9)$$

$$P_{i,t}^{DG} = P_{i,t}^{DG\max} \forall i \in \Omega^{DGN}, \forall t \in T, \quad (10)$$

$$Q_{i,t}^{DG} = P_{i,t}^{DG} \tan \varphi \forall i \in \Omega^{DGN}, \forall t \in T, \quad (11)$$

$$\tilde{U}_{i\min} \leq \tilde{U}_{i,t} \leq \tilde{U}_{i\max} \forall i \in \Omega^{node}, \forall t \in T. \quad (12)$$

Constraint (8) limits the transmission power capacity of the root node. Constraint (9) represents the feeder capacity constraint. Then, curtailment constraints with respect to distributed generation are given in **10, 11**. Constraint (12) limits the operating range of the squared voltage magnitude.

ESS operation constraints include charge and discharge state constraints, storage capacity constraints, charge and discharge

power constraints, and daily allowable charge and discharge times constraints (Gabash and Li, 2012), which are provided as follows:

$$y_{i,t}^{ch} + y_{i,t}^{dis} \leq 1, \forall i \in \Omega^{ESS}, \forall t \in T, \quad (13)$$

$$\begin{cases} 0 \leq P_{i,t}^{dis} \leq y_{i,t}^{dis} P_{max}^e \\ 0 \leq P_{i,t}^{ch} \leq y_{i,t}^{ch} P_{max}^e \end{cases}, \forall i \in \Omega^{ESS}, \forall t \in T, \quad (14)$$

$$\begin{cases} E_{i,t+1}^{ESS} = E_{i,t}^{ESS} + \alpha P_{i,t}^{ch} - \beta P_{i,t}^{dis} \\ 0.2E_i^{max} \leq E_{i,t}^{ESS} \leq 0.9E_i^{max} \end{cases}, \forall i \in \Omega^{ESS}, \forall t \in T, \quad (15)$$

$$\begin{cases} \sum_t |y_{i,t+1}^{ch} - y_{i,t}^{ch}| \leq \lambda_{max}^{ESS} \\ \sum_t |y_{i,t+1}^{dis} - y_{i,t}^{dis}| \leq \lambda_{max}^{ESS} \end{cases}, \forall i \in \Omega^{ESS}, \forall t \in T. \quad (16)$$

Constraint (13) denotes the charging and discharging states of ESS, and constraint (14) represents upper limit of charge and discharge. Eqs 15, 16 are energy constraints of ESS and daily allowable charge and discharge times constraints, respectively. Then, the quadratic equality (5) is further relaxed into the following SOC inequality (Taylor and Hover, 2012; Farivar and Low, 2013):

$$\left\| \begin{bmatrix} 2P_{ij,t} \\ 2Q_{ij,t} \\ \tilde{I}_{ij,t} - \tilde{U}_{ij,t} \end{bmatrix} \right\|_2 \leq \tilde{I}_{ij,t} + \tilde{U}_{ij,t}, \forall i \in \Omega^{node} \forall j \in \Omega^{line}, \forall t \in T, \quad (17)$$

where $\|\cdot\|_2$ is the mathematical expression of the Euclid norm.

2.2 Model of the Energy Hub

The EH (Chen et al., 2019) depicted in Figure 1A represents the coupling between electricity and gas networks. CHP represents the key component of this EH, which generates electricity and heat simultaneously, and the urban distribution network provides the charging service for EVs through the EH. The energy conversion efficiency between the input and output energy flows of the EH is formulated in 18

$$\begin{bmatrix} L_{i,t}^e \\ L_{i,t}^h \end{bmatrix} = \begin{bmatrix} \eta_{ee} & \nu \eta_{CHP,e} \\ 0 & \nu \eta_{CHP,h} + (1-\nu) \eta_{gh} \end{bmatrix} \begin{bmatrix} P_{i,t}^{EH} \\ F_{i,t}^{EH} \end{bmatrix}. \quad (18)$$

Eq. 19 represents the dispatch factor of the EH input gas flow

$$0 \leq \nu \leq 1. \quad (19)$$

Then, the EH also needs to satisfy the following operating constraints:

$$F_{EH,min} \leq F_{i,t}^{EH} \leq F_{EH,max}, \quad (20)$$

$$S_{chp,min} \leq \nu F_{i,t}^{EH} \leq S_{chp,max}, \quad (21)$$

$$S_{gf,min} \leq (1-\nu) F_{i,t}^{EH} \leq S_{gf,max}. \quad (22)$$

Constraint (20) gives the range of total gas purchases of EH. Constraints (20) and (21) represent the production capacity of CHP units and gas furnaces, respectively.

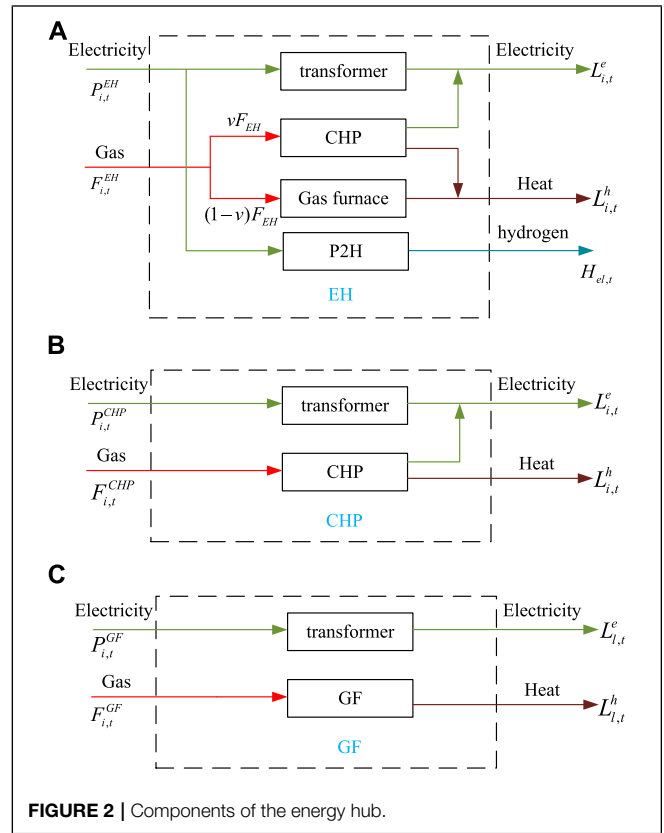


FIGURE 2 | Components of the energy hub.

For a specific case, the nodes of the distribution network are connected to some components of EH, for example, only CHP units or gas furnaces, as shown in Figure 2. On the other hand, the power distribution network converts electric power into hydrogen through P2H devices to provide hydrogen supply services for hydrogen-fueled vehicles on the traffic side (Korpas and Holen, 2006; Pan et al., 2021). The structure of P2H is shown in Figure 3.

The energy conversion efficiency between the input and output energy flows of P2H is given in 23 and 24

$$H_{el,t} = \eta_{e2hy} P_{i,t}^{P2H} \Delta t / H_c, \quad (23)$$

$$0 \leq H_{el,t} \leq H_{el}^{max}. \quad (24)$$

Constraint (23) calculates the energy conversion efficiency between the input and output energy flows of P2H. Constraint (24) limits the hydrogen production.

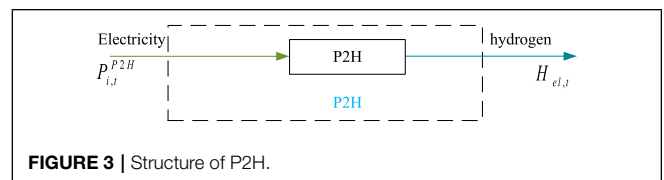


FIGURE 3 | Structure of P2H.

2.3 Transportation System Modeling

The user equilibrium (UE) model has been widely used to describe the urban transportation system in transportation research. In the case of the given traffic network and traffic demand, the UE model can output the current traffic state, namely, the traffic flow distribution on the road. The transportation system model in this article is based on the mixed-UE traffic flow model (Wei et al., 2018). We divide the overall vehicular flows into five categories: GV traffic flow, EV traffic flow, HV traffic flow, HV charging flow, and EV charging flow. The difference between traffic flow and charging flow lies in that the former represents the route choice of EVs and HVs, while the latter represents the charging choice of EVs and HVs. Traffic link has regular link, charging link, and bypass link. The charging links correspond to EV and HV queuing and charging events in EVCs and HVCs, and bypass links denote bypass events at EVCs and HVCs (Lv et al., 2021b; Teng et al., 2021).

The improved mixed-UE transportation model is a nonlinear complementary problem (NCP) consisting of four constraint sets

$$UE - NCP \begin{cases} Cons - Flow, Cons - Time \\ Cons - Cost, Cons - CP \end{cases} \quad (25)$$

where constraint sets are presented as follows:

Cons - Flow:

$$\sum_{\rho \in \lambda_g^{rs}} f_{\rho,rs,t}^g = \pi^g q_{rs,t}, \quad (26)$$

$$\sum_{\rho \in \lambda_e^{rs}} f_{\rho,rs,t}^e = \pi^e q_{rs,t}, \quad (27)$$

$$\sum_{\rho \in \lambda_h^{rs}} f_{\rho,rs,t}^h = \pi^h q_{rs,t}, \quad (28)$$

$$x_{a,t}^g = \sum_{rs \in \lambda_g^a} \sum_{\rho \in \lambda_g^{rs}} f_{\rho,rs,t}^g \delta_{a,\rho,rs}^g + \sum_{rs \in \lambda_e^a} \sum_{\rho \in \lambda_e^{rs}} f_{\rho,rs,t}^e \delta_{a,\rho,rs}^e + \sum_{rs \in \lambda_h^a} \sum_{\rho \in \lambda_h^{rs}} f_{\rho,rs,t}^h \delta_{a,\rho,rs}^h, \quad (29)$$

$$x_{a,t}^e = \sum_{rs \in \lambda_e^a} \sum_{\rho \in \lambda_e^{rs}} f_{\rho,rs,t}^e \delta_{a,\rho,rs}^e, \quad (30)$$

$$x_{a,t}^h = \sum_{rs \in \lambda_h^a} \sum_{\rho \in \lambda_h^{rs}} f_{\rho,rs,t}^h \delta_{a,\rho,rs}^h, \quad (31)$$

$$\pi^g + \pi^e + \pi^h = 1, \pi^g, \pi^e, \pi^h > 0. \quad (32)$$

Cons - Time:

$$t_{a,t}^{rg} = t_a^0 \left[1 + 0.15 \left(\frac{x_{a,t}^g}{c_a^{rg}} \right)^4 \right], \quad (33)$$

$$t_{a,t}^{che} = \frac{E^e}{P_{ser,e}} + t_{a,che}^{\max} \left(\frac{x_{a,t}^e}{c_a^{che}} \right)^3, x_{a,t}^e \leq c_a^{che}, \quad (34)$$

$$t_{a,t}^{chh} = \frac{E^h}{P_{ser,h}} + t_{a,chh}^{\max} \left(\frac{x_{a,t}^h}{c_a^{chh}} \right)^3, x_{a,t}^h \leq c_a^{chh}. \quad (35)$$

Cons - Cost:

$$c_{\rho,rs,t}^g = \sum_a \omega_{a,t}^{rg} \delta_{a,\rho,rs}^g, \quad (36)$$

$$c_{\rho,rs,t}^e = \sum_a \omega_{a,t}^{re} \delta_{a,\rho,rs}^e + \sum_a (\omega_{a,t}^{che} + \lambda_{a,t}^e E^e) \delta_{a,\rho,rs}^e, \quad (37)$$

$$c_{\rho,rs,t}^h = \sum_a \omega_{a,t}^{rh} \delta_{a,\rho,rs}^h + \sum_a (\omega_{a,t}^{chh} + \lambda_{a,t}^h E^h) \delta_{a,\rho,rs}^h. \quad (38)$$

Cons - Cp:

$$0 \leq f_{\rho,rs,t}^g \perp c_{\rho,rs,t}^g - u_{rs,t}^g \geq 0, \quad (39)$$

$$0 \leq f_{\rho,rs,t}^e \perp c_{\rho,rs,t}^e - u_{rs,t}^e \geq 0, \quad (40)$$

$$0 \leq f_{\rho,rs,t}^h \perp c_{\rho,rs,t}^h - u_{rs,t}^h \geq 0. \quad (41)$$

Constraint set *Cons - Flow* describes flow conservation in the TN. Specifically, constraints (29)–(31) indicate that the traffic flow on each link is equal to the sum of the flows on all paths that pass through the link. Constraints (26)–(28) explain that the traffic flow on all paths connecting each O-D pair is equal to the corresponding traffic demand. Constraint set *Cons - Time* gives link travel time and estimation of different link types, respectively. For regular link $a \in T_A^{rg}$, constraint (33) uses the Bureau of Public Roads (BPR) function [Bureau of Public Roads (1, 1964)] to represent the link travel time as a function of x_a^g . In constraint (7), the first and second terms denote the charging time and queuing time, respectively. Constraint set *Cons - Cost* describes the travel costs of GVs, EVs, and HVs that choose path ρ . Note that the cost for EVs and HVs contains both travel cost and charging cost, respectively. Constraint set *Cons - Cp* represents the complementarity condition of the Wardrop UE principle (Sheffi, 1985), which indicates that no GV/EV/HV travelers could decrease their travel costs by unilaterally switching their route choices.

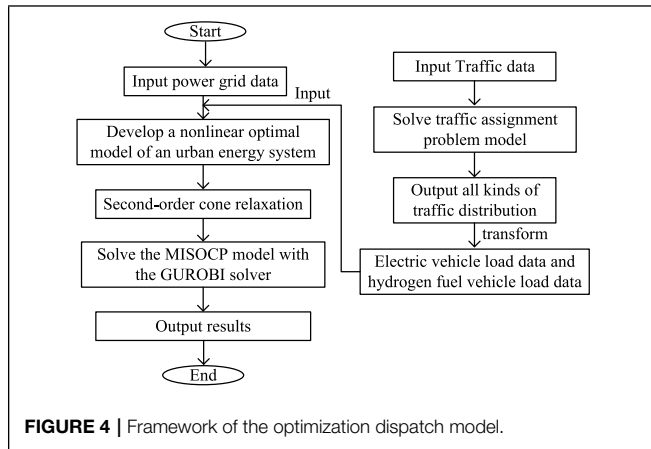
By changing the electricity price and hydrogen price for each period of time, we calculate the transportation network model 24 times. Then, we can get the load curve of each charging station and hydrogen charging station in a day according to **Eqs 42, 43**. In addition, the heat load $L_{i,t}^h$ can be obtained from the literature (Soroudi, 2017)

$$L_{i,t}^e = E^e x_{a,t}^e, \quad (42)$$

$$L_{i,t}^h = E^h x_{a,t}^h. \quad (43)$$

2.4 The Day-Ahead Optimization Dispatch Model of an Urban Energy System

With the goal of minimizing the sum of gas purchase cost and electricity purchase cost, we established a day-ahead optimization dispatch model of an urban energy system, and the



optimization model is summarized below (Lu et al., 2020; Bakeer and Hossam, 2021; Cheng et al., 2021; Lu et al., 2020; Bakeer and Hossam, 2021; Cheng et al., 2021).

The objective function is provided as

$$\min \mu_{e,t} P_{i,t}^{sub} + \mu_{g,t} (F_{i,t}^{EH} + F_{i,t}^{CHP} + F_{i,t}^{GF}). \quad (44)$$

The objective function (44) is subject to Day-ahead operation

$$\text{constraints: } \begin{cases} (1) - (4) \\ (6) - (17) \\ (18) - (24) \\ (42) - (43) \end{cases}$$

Figure 4 shows the framework of the day-ahead optimization dispatch model of an urban energy system, which clarifies the interactions between power and transportation networks from the modeling perspective.

3 CASE STUDY

The urban energy system shown in Figure 5 is composed of a transportation network and a 33-node urban electricity network with five EHs located at nodes 6, 16, 18, 21, and 30 and two P2H units at nodes 8 and 10. CS1–CS8 are charging stations which correspond to nodes 6, 16, 12, 27, 18, 25, 21, and 30 in the power network, respectively. HFS1–HFS7 are hydrogen charging stations which correspond to nodes 6, 16, 21, 30, 18, 10, and 8 in the power network, respectively. In addition, two 0.4-MW capacity wind farms are connected at nodes 14 and 33, while two 1.8-MW capacity ESSs are connected at nodes 11 and 29, respectively. The computational tests were conducted on a laptop with Intel Core i7 CPU and 16 GB memory, and the MISOCP model was programmed in GAMS and solved with the GUROBI solver.

3.1 Electric Vehicle Charging Load and Hydrogen Load

Figure 6 shows the daily heat load, the charging load of EVs, and the hydrogen load of HVs on the traffic side. As can be observed from this figure, the charging load curve of EVs has the same trend with the hydrogen load curve of HVs, and both have the

characteristic of double peaks. During the morning rush hour from 8:00 to 10:00 and the evening rush hour from 17:00 to 19:00, the electric load and hydrogen load on the traffic side are relatively high, while the heat load is higher during the day and lower at night (Ye et al., 2021). The trend of these three loads is consistent with that of the total load.

3.2 The Anti-Peak-Shaving Characteristic of Wind Power Production

Figure 7 shows the comparison of the wind power output curve, total original load curve, and total net load curve without considering energy storage. In this figure, load 0 represents the total original load curve, and load 1 represents the total net load curve without considering the energy storage. As can be observed from the figure, wind turbines produce more output at night, which results in a lower net load at the valley time. However, the output of wind turbines is less in the daytime, and hence, it cannot significantly reduce the peak load. Consequently, the daily wind power production results in a larger peak-to-valley difference of net load.

3.3 Coordination Between ESS and Wind Power Production

It is noteworthy that when the ESS participates in the power regulation of the power grid, the disadvantages brought by the anti-peak-shaving of wind power can be well compensated. As shown in Figure 8, load 3 represents the total net load considering energy storage and multi-energy regulation, and load 2 represents the total net load without considering multi-energy regulation. ESS charges at night when the power load is low and the wind power output is large and discharges during the day when the load is relatively high and the wind power output is small. As a result, peak cutting and valley filling of the power load are achieved.

3.4 Complementary Operation of Multi-Energy Coupling

Natural gas is simultaneously converted into heat and electricity through CHP units and only into heat through the gas furnace. Figure 9 shows the total purchase of natural gas at each time period, from which we can observe that the amount of gas purchase of gas is larger at the time period when the power load is high than that at the time period when the power load is low. As shown in Figure 8, the difference between curve load 2 and load 3 is mainly due to the multi-energy complement. In addition, the EV load is relatively high at time periods from 7:00 to 17:00. To summarize, increasing the power supply of CHP units can effectively reduce the peak load, but this impact on valley filling is not obvious.

3.5 Impact of ESS Strategies on Urban Energy System Operation

As discussed above, ESS can play an important role in power systems. Reasonable ESS scheduling decisions can alleviate the impact of wind power on the distribution network and promote

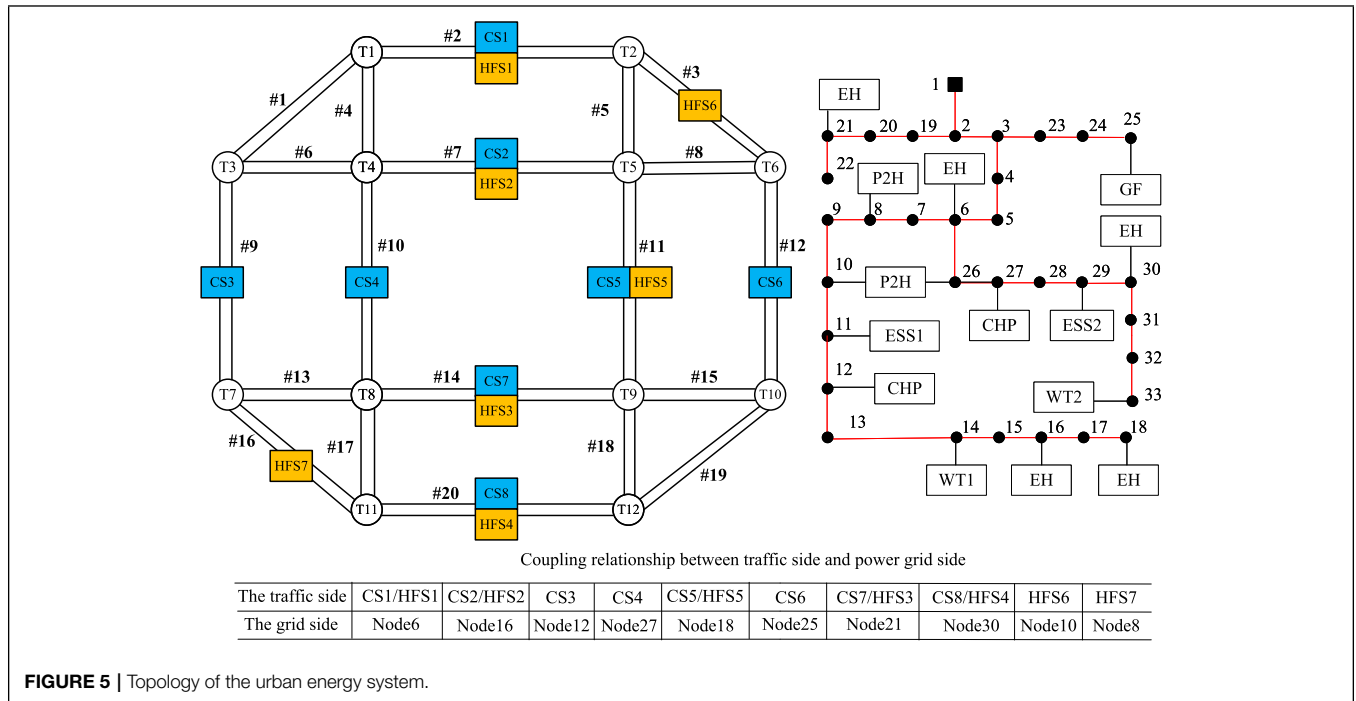


FIGURE 5 | Topology of the urban energy system.

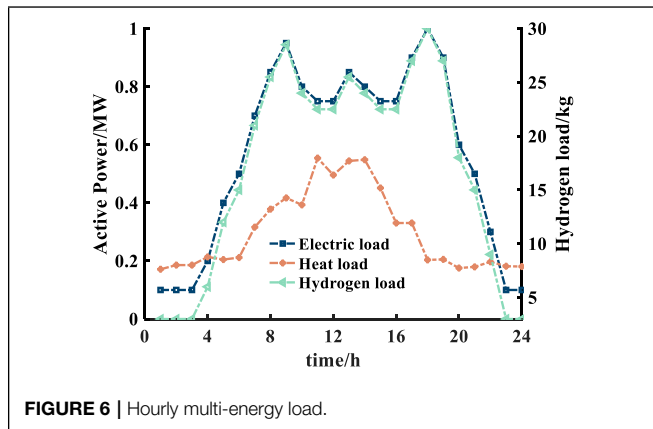


FIGURE 6 | Hourly multi-energy load.

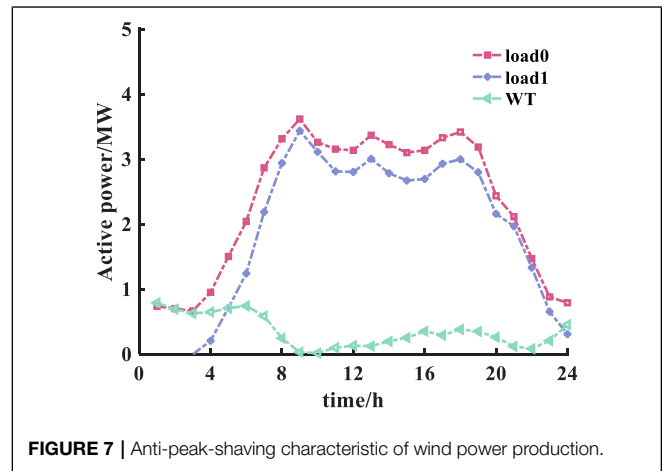


FIGURE 7 | Anti-peak-shaving characteristic of wind power production.

peak shaving and valley filling. **Figure 10** and **Figure 11** show the charge–discharge curve of ESS and the SOC state of charge of ESS, respectively. We can note that for time periods from 0:00 to 7:00, the net load is relatively with low power consumption and high wind power production, and ESS charges to satisfy the load electricity demand. The SOC state of charge rises in preparation for the next stage of the discharge process. For time periods from 8:00 to 11:00, the electricity price is high and the net load is relatively high. ESS reduces the load peak by discharging. From 16:00 to 19:00, the load reaches the peak again, and ESS continues to discharge, which reduces the power purchase cost from the main grid. At the same time, in order to ensure the normal operation of the next charge and discharge cycle, the ESS charges and returns to the original state of charge at time periods from 20:00 to 24:00.

We introduce an index δP_a to measure the average peak-valley difference:

$$\delta P_a = \sum_{t_{peak}} P_{i,t_{peak}} / N_{peak} - \sum_{t_{valley}} P_{i,t_{valley}} / N_{valley}. \quad (45)$$

Table 1 lists mean peak-valley differences and the total operation costs under different ESS capacities. As shown in this table, the increase in ESS capacity positively reduces the average peak-valley difference of power demands and reduces the total operating costs. This is because a higher energy storage capacity can provide more sufficient charging power in load valley and discharging power in load peak, which also reduces the purchase of power at the peak time, thus reducing the operating cost.

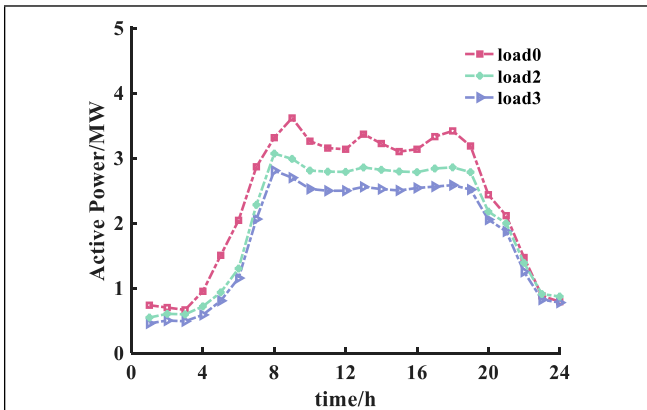


FIGURE 8 | Hourly load curves under three scenarios.

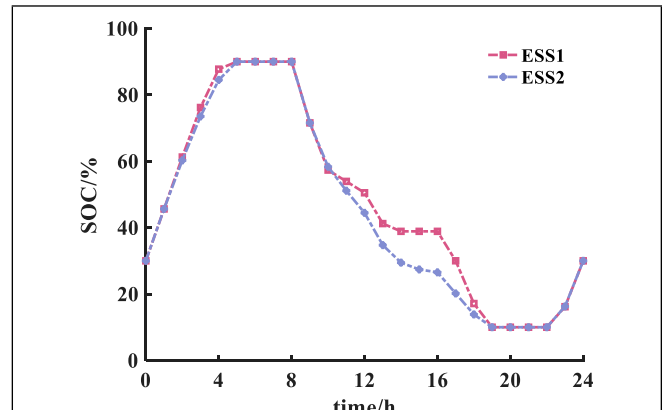


FIGURE 11 | Hourly SOC state of charge of ESS.

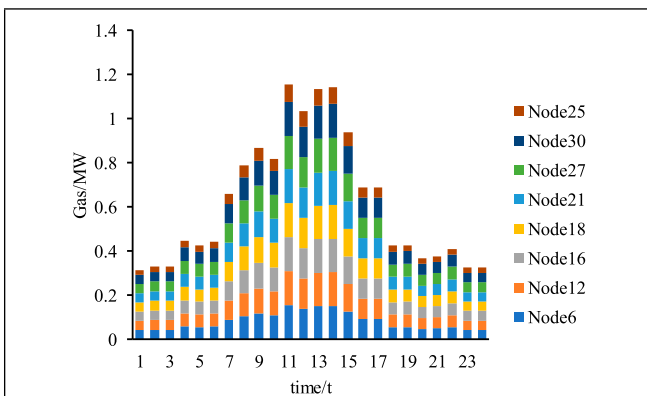


FIGURE 9 | Hourly total purchase of natural gas.

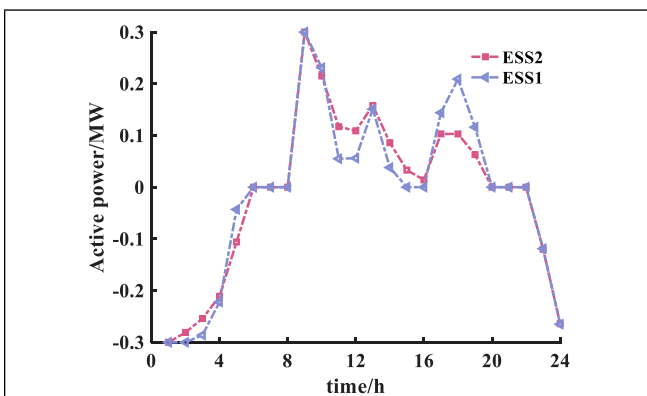


FIGURE 10 | Hourly charge-discharge curve of ESS.

TABLE 2 | Cost comparison under different constraint values of average peak-valley difference.

λ /MW	1.37	1.27	1.15	1.10	1.05
Cost/\$	25145.35	25282.07	25731.15	25952.80	26179.76

3.6 Cost Comparison Under Different Values of Average Peak-Valley Difference

To control the load peak-valley difference to an ideal level, we add an additional linear constraint (46) into the original model. Meanwhile, we set the energy storage capacity to be fixed at the original value

$$\delta P_a \leq \lambda. \tag{46}$$

λ denotes the load peak-valley difference which we want to get. By modifying the value of λ , we can obtain the corresponding operating costs under different requirements of average peak-valley difference, and the results are summarized in Table 2.

Generally, a more ideal peak-valley difference increases the total operating cost, which indicates that the operating cost and the requirement of peak shaving and valley filling are contradictory. The reason is that if we set the value of λ to be small, we need to increase the net load during the valley time. Therefore, part of the wind power will be curtailed during the load valley, and additional electricity needs to be purchased from the main grid, which reduces the peak-to-valley difference and inevitably increase the total operating cost.

TABLE 1 | Average peak-valley difference under different ESS capacities.

Capacity of ESS/MW	1.8	2.2	2.6	2.8	3.2
Mean peak-valley difference/MW	1.37	1.27	1.16	1.11	1.00
Cost/\$	25145.35	25029.00	24919.91	24868.68	24778.03

4 CONCLUSION

We have presented a day-ahead co-optimization approach of urban energy systems considering traffic flows and peak shaving. Based on the numerical results obtained, we can draw the following conclusions:

- Optimal charging and discharging dispatch strategies of energy storages can alleviate the peak-valley difference caused by the anti-peak-shaving characteristic of wind power production.
- In addition, multi-energy complement can significantly reduce the peak-valley difference and contribute to the improved energy utilization efficiency. However, increasing the supply of natural gas can reduce the peak load, but the effect on valley filling is not obvious.
- When the ESS capacity is fixed, the higher the peak shaving and valley filling requirements, the greater the operating cost.

Our work, hence, might help the operators of urban energy systems to produce operating decisions of multi-energy production sources and satisfy the requirement from multi-energy demands. Our work might also help the design of a future low-carbon energy system. Meanwhile, in future research, we will consider the optimal dispatch model of the transportation system into the day-ahead dispatch model of the urban energy system to further improve social benefits. Reasonable traffic management strategies can give

REFERENCES

- Bakeer, A., and Hossam, S. (2021). Salama and Istvan Vokony. Integration of PV System with SMES Based on Model Predictive Control for Utility Grid Reliability Improvement. *Prot. Control. Mod. Power Syst.* 6 (2), 191–203. doi:10.1186/s41601-021-00191-1
- Baran, M. E., and Wu, F. F. (1989). Network Reconfiguration in Distribution Systems for Loss Reduction and Load Balancing. *IEEE Trans. Power Deliv.* 4 (2), 1401–1407. doi:10.1109/61.25627
- Bureau of Public Roads (1964). *Traffic Assignment Manual*. Washington, D.C.: U.S. Department of Commerce.
- Chen, S., Wei, Z., Sun, G., Cheung, K. W., Wang, D., and Zang, H. (2019). Adaptive Robust Day-Ahead Dispatch for Urban Energy Systems. *IEEE Trans. Ind. Electron.* 66 (2), 1379–1390. doi:10.1109/tie.2017.2787605
- Chen, Y., Gribik, P., and Gardner, J. (2014). Incorporating Post Zonal Reserve Deployment Transmission Constraints into Energy and Ancillary Service Co-optimization. *IEEE Trans. Power Syst.* 29 (2), 537–549. doi:10.1109/tpwrs.2013.2284791
- Cheng, Yan., Tang, Yi., and Dai, Jianfeng. (2021). Uncertainty Modeling of Wind Power Frequency Regulation Potential Considering Distributed Characteristics of Forecast Errors. *Prot. Control. Mod. Power Syst.* 6 (3), 276–288.
- Correa-Posada, C. M., and Sánchez-Martín, P. (2015). Integrated Power and Natural Gas Model for Energy Adequacy in Short-Term Operation. *IEEE Trans. Power Syst.* 30 (6), 3347–3355. doi:10.1109/tpwrs.2014.2372013
- Farivar, M., and Low, S. H. (2013). Branch Flow Model: Relaxations and Convexification-Part I. *IEEE Trans. Power Syst.* 28 (3), 2554–2564. doi:10.1109/tpwrs.2013.2255317
- Gabash, A., and Li, P. (2012). Active-Reactive Optimal Power Flow in Distribution Networks with Embedded Generation and Battery Storage. *IEEE Trans. Power Syst.* 27 (4), 2026–2035. doi:10.1109/tpwrs.2012.2187315

full play to the initiative of the urban distribution network to achieve peak shaving and valley filling and economic optimization.

DATA AVAILABILITY STATEMENT

The original contributions presented in the study are included in the article/Supplementary Materials, further inquiries can be directed to the corresponding author.

AUTHOR CONTRIBUTIONS

YP: methodology, software, validation, formal analysis, writing—original draft, and visualization. JM: methodology, investigation, and writing—review editing. CL conceptualization, methodology, and writing—review editing. SC conceptualization, resources, and supervision. LP methodology, validation, and writing—review editing.

FUNDING

This work was supported by State Grid Zhejiang Electric Power Company Project “Steady-state models and parameter identification technology of energy storage stations”.

- Gao, H., and Li, Z. (2021). A Benders Decomposition Based Algorithm for Steady-State Dispatch Problem in an Integrated Electricity-Gas System. *IEEE Trans. Power Syst.* 36 (4), 3817–3820. doi:10.1109/tpwrs.2021.3067203
- Gao, H., and Li, Z. (2020). “Effect of Power to Gas on Integrated Electricity-Gas System with Uncertain Wind Generation,” in IEEE 3rd Student Conference on Electrical Machines and Systems. SCEMS, 164–168. doi:10.1109/scems48876.2020.9352402
- Hu, X., Moura, S. J., Murgovski, N., Egardt, B., and Cao, D. (2016). Integrated Optimization of Battery Sizing, Charging, and Power Management in Plug-In Hybrid Electric Vehicles. *IEEE Trans. Contr. Syst. Technol.* 24 (3), 1036–1043. doi:10.1109/tcst.2015.2476799
- IEA, Global EV Outlook (2020). *Entering the Decade of Electric Drive?* International Energy Agency.
- Jin, X., Mu, Y., Jia, H., Wu, J., Xu, X., and Yu, X. (2016). Optimal Day-Ahead Scheduling of Integrated Urban Energy Systems. *Appl. Energy.* 180, 1–13. doi:10.1016/j.apenergy.2016.07.071
- Korpas, M., and Holen, A. T. (2006). Operation Planning of Hydrogen Storage Connected to Wind Power Operating in a Power Market. *IEEE Trans. Energy Convers.* 21 (3), 742–749. doi:10.1109/tec.2006.878245
- Li, Y., Zou, Y., Tan, Y., Cao, Y., Liu, X., Shahidehpour, M., et al. (2018). Optimal Stochastic Operation of Integrated Low-Carbon Electric Power, Natural Gas, and Heat Delivery System. *IEEE Trans. Sustain. Energy.* 9 (1), 273–283. doi:10.1109/tste.2017.2728098
- Lu, S., Gu, W., Meng, K., Yao, S., Liu, B., and Dong, Z. Y. (2020). Thermal Inertial Aggregation Model for Integrated Energy Systems. *IEEE Trans. Power Syst.* 35 (3), 2374–2387. doi:10.1109/tpwrs.2019.2951719
- Lv, S., Chen, S., Wei, Z., and Zhang, H. (2021). Power Transportation Coordination: toward a Hybrid Economic-Emission Dispatch Model. *IEEE Trans. Power Syst.* doi:10.1109/tpwrs.2021.3131306
- Lv, S., Wei, Z., Chen, S., Sun, G., and Wang, D. (2021). Integrated Demand Response for Congestion Alleviation in Coupled Power and Transportation

- Networks. *Appl. Energ.* 283, 116206. doi:10.1016/j.apenergy.2020.116206
- Mancarella, P. (2014). MES (Multi-energy Systems): An Overview of Concepts and Evaluation Models. *Energy* 65, 1–17. doi:10.1016/j.energy.2013.10.041
- Martínez-Mares, A., Fuerte-Esquivel, C. R., and de Ingeniería, I. (2011). *Integrated Energy Flow Analysis in Natural Gas and Electricity Coupled Systems*. North American Power Symposium, 1–7.
- Meng, W., and Wang, X. (2017). Distributed Energy Management in Smart Grid with Wind Power and Temporally Coupled Constraints. *IEEE Trans. Ind. Electron.* 64 (8), 6052–6062. doi:10.1109/tie.2017.2682001
- Neyestani, N., Yazdani-Damavandi, M., Shafie-khah, M., Chicco, G., and Catalao, J. P. S. (2015). Stochastic Modeling of Multienergy Carriers Dependencies in Smart Local Networks with Distributed Energy Resources. *IEEE Trans. Smart Grid* 6 (4), 1748–1762. doi:10.1109/tsg.2015.2423552
- Pan, G., Hu, Q., Gu, W., Ding, S., Qiu, H., and Lu, Y. (2021). Assessment of Plum Rain's Impact on Power System Emissions in Yangtze-Huaihe River basin of China. *Nat. Commun.* 12, 6156. doi:10.1038/s41467-021-26358-w
- Rotering, N., and Ilic, M. (2011). Optimal Charge Control of Plug-In Hybrid Electric Vehicles in Deregulated Electricity Markets. *IEEE Trans. Power Syst.* 26 (3), 1021–1029. doi:10.1109/tpwrs.2010.2086083
- Saber, A. Y., and Venayagamoorthy, G. K. (2011). Plug-in Vehicles and Renewable Energy Sources for Cost and Emission Reductions. *IEEE Trans. Ind. Electron.* 58 (4), 1229–1238. doi:10.1109/tie.2010.2047828
- Shabanpour-Haghighi, A., and Seifi, A. R. (2015). Energy Flow Optimization in Multicarrier Systems. *IEEE Trans. Ind. Inf.* 11 (5), 1067–1077. doi:10.1109/tii.2015.2462316
- Sheffi, Y. (1985). *Urban Transportation Networks: Equilibrium Analysis with Mathematical Programming Methods*. Englewood Cliffs, NJ, USA: Prentice-Hall.
- Soroudi, A. (2017). *Power System Optimization Modeling in GAMS*.
- Strasser, T., Andren, F., Kathan, J., Cecati, C., Buccella, C., Siano, P., et al. (2015). A Review of Architectures and Concepts for Intelligence in Future Electric Energy Systems. *IEEE Trans. Ind. Electron.* 62 (4), 2424–2438. doi:10.1109/tie.2014.2361486
- Taylor, J. A., and Hover, F. S. (2012). Convex Models of Distribution System Reconfiguration. *IEEE Trans. Power Syst.* 27 (3), 1407–1413. doi:10.1109/tpwrs.2012.2184307
- Teng, W., Wang, Y., and Sun, S. (2021). Robust Stability Control for Electric Vehicles Connected to DC Distribution Systems. *Front. Energ. Res.* 9. doi:10.3389/fenrg.2021.740698
- Uddin, M., Romlie, M. F., Abdullah, M. F., Abd Halim, S., Abu Bakar, A. H., and Chia Kwang, T. (2018). A Review on Peak Load Shaving Strategies. *Renew. Sustain. Energ. Rev.* 82, 3323–3332. doi:10.1016/j.rser.2017.10.056
- Wei, W., Wu, L., Wang, J., and Mei, S. (2018). Network Equilibrium of Coupled Transportation and Power Distribution Systems. *IEEE Trans. Smart Grid* 9 (6), 6764–6779. doi:10.1109/tsg.2017.2723016
- Xu, D., Wu, Q., Zhou, B., Li, C., Bai, L., and Huang, S. (2020). Distributed Multi-Energy Operation of Coupled Electricity, Heating, and Natural Gas Networks. *IEEE Trans. Sustain. Energ.* 11 (4), 2457–2469. doi:10.1109/tste.2019.2961432
- Yang, Q., and Fang, X. (2017). Demand Response under Real-time Pricing for Domestic Households with Renewable DGs and Storage. *IET Generation, Transm. Distribution* 11 (8), 1910–1918. doi:10.1049/iet-gtd.2016.1066
- Ye, J., Zhao, D., and Zhang, L. (2021). Research on Combined Electricity and Heating System Scheduling Method Considering Multi-Source Ring Heating Network. *Front. Energ. Res.* 9. doi:10.3389/fenrg.2021.800906
- Zhao, G. Y., Liu, Z. Y., He, Y., Cao, H. J., and Guo, Y. B. (2017). Energy Consumption in Machining: Classification, Prediction, and Reduction Strategy. *Energy* 133, 142–157. doi:10.1016/j.energy.2017.05.110
- Zhao, J., Ma, Y., Liu, Q., Wen, L., Jia, C., and Fang, Y. (2020). A Multi-Source Coordinated Optimal Operation Model Considering the Risk of Nuclear Power Peak Shaving and Wind Power Consumption. *IEEE Access* 8, 189702–189719. doi:10.1109/access.2020.3027705

Conflict of Interest: The authors declare that the research was conducted in the absence of any commercial or financial relationships that could be construed as a potential conflict of interest.

Publisher's Note: All claims expressed in this article are solely those of the authors and do not necessarily represent those of their affiliated organizations or those of the publisher, the editors, and the reviewers. Any product that may be evaluated in this article or claim that may be made by its manufacturer is not guaranteed or endorsed by the publisher.

Copyright © 2022 Peng, Ma, Lu, Chen and Pei. This is an open-access article distributed under the terms of the Creative Commons Attribution License (CC BY). The use, distribution or reproduction in other forums is permitted, provided the original author(s) and the copyright owner(s) are credited and that the original publication in this journal is cited, in accordance with accepted academic practice. No use, distribution or reproduction is permitted which does not comply with these terms.

GLOSSARY

Indices and sets

- i, j Subscript indices of nodes in electricity networks
- t Subscript indices of time periods
- min Superscript index of minimum value
- max Superscript index of maximum value
- Ω^{node} Set of electrical nodes
- Ω^{line} Set of branches
- Ω^{sub} Set of root nodes
- Ω^{ESS} Set of (energy storage system) ESS nodes
- Ω^{DGN} Set of DG nodes
- T Operational cycle.
- T_A^{rg} Set of regular links in a transportation network.
- T_A^{ch} Set of charging links in the transportation network
- T_{RS} Set of origin–destination (O-D) pairs
- T_R Set of origin nodes
- T_S Set of destination nodes.
- $\lambda_g^{rs}, \lambda_e^{rs}, \lambda_h^{rs}$ Set of gasoline vehicles/electric vehicles/hydrogen fuel vehicles (GV/EV/HV) paths connecting an O-D pair r-s, where $r \in T_{RS}, s \in T_S$ and $rs \in T_{RS}$

Variables

- $U_{i,t}$ Voltage of electrical nodes
- $I_{ij,t}$ Current magnitude through branch ij
- $P_{ij,t}, Q_{ij,t}$ Active and reactive power flow through branch ij
- $P_{i,t}^{inj}, Q_{i,t}^{inj}$ The injected active and reactive power of node i
- $P_{i,t}^{sub}, Q_{i,t}^{sub}$ Output active and reactive power of the root node
- $P_{i,t}^{DG}, Q_{i,t}^{DG}$ Output active and reactive power of the distributed generation
- $P_{i,t}^L, Q_{i,t}^L$ Active and reactive power load
- $P_{i,t}^{ch}, P_{i,t}^{dis}$ Active power charge and discharge of ESS
- $P_{i,t}^{EH}$ Input power flow of the energy hub (EH)
- $P_{i,t}^{GF}$ Input power flow of the gas furnace (GF)
- $P_{i,t}^{CHP}$ Input power flow of combined heat and power (CHP)
- $P_{i,t}^{P2H}$ Input power flow of power to hydrogen (P2H)
- $y_{i,t}^{ch}, y_{i,t}^{dis}$ Binary variable
- $E_{i,t}^{ESS}$ Energy level of the ESS
- $L_{i,t}^e, L_{i,t}^h$ Dispatched electricity and heat demand
- $F_{i,t}^{EH}$ Input gas flow of the energy hub
- v Percentage of gas fed into combined heat and power
- $H_{el,t}$ Hydrogen production
- $f_{\rho,rs,t}^g$ GV flow on path $\rho \in \lambda_g^{rs}$ between O-D pair r-s
- $f_{\rho,rs,t}^e$ EV flow on path $\rho \in \lambda_e^{rs}$ between O-D pair r-s
- $f_{\rho,rs,t}^h$ HV flow on path $\rho \in \lambda_h^{rs}$ between O-D pair r-s

- $x_{a,t}^e$ Aggregated traffic flow on link $a \in T_A^{ch}$
- $x_{a,t}^g$ Aggregated traffic flow on link $a \in T_A^{rg}$
- $x_{a,t}^h$ Aggregated traffic flow on link $a \in T_A^{ch}$
- $t_{a,t}^{rg}$ Travel time on link $a \in T_A^{rg}$
- $t_{a,t}^{ch,e}$ Average time that EVs spend on link $a \in T_A^{ch}$
- $t_{a,t}^{ch,h}$ Average time that HVs spend on link $a \in T_A^{ch}$
- $c_{\rho,rs,t}^g$ GV travel cost on path $\rho \in \lambda_g^{rs}$ between O-D pair r-s
- $c_{\rho,rs,t}^e$ EV travel cost on path $\rho \in \lambda_e^{rs}$ between O-D pair r-s
- $c_{\rho,rs,t}^h$ HV travel cost on path $\rho \in \lambda_h^{rs}$ between O-D pair r-s
- $u_{rs,t}^g$ Minimal travel cost of GVs between O-D pair r-s
- $u_{rs,t}^e$ Minimal travel cost of EVs between O-D pair r-s
- $u_{rs,t}^h$ Minimal travel cost of HVs between O-D pair r-s
- $P_{i,t}^{peak}, P_{i,t}^{valley}$ Peak and valley net load

Parameters

- $R_{ij,t}$ The resistance of branch ij
- $X_{ij,t}$ The reactance of branch ij
- $\tan \varphi$ Power factor of DG output
- P_{max}^e Upper limits of ESS charge and discharge power
- α, β Charge and discharge efficiency coefficient of ESS
- E_i^{max} Maximum storage capacity of ESS
- λ_{max}^{ESS} Maximum charging and discharging times of ESS
- η_{ee} Transformer efficiency of the energy hub
- $\eta_{CHP,e}$ Electrical efficiency of combined heat and power
- $\eta_{CHP,h}$ Thermal efficiency of combined heat and power
- η_{gh} Gas furnace efficiency
- η_{e2hy} Electrical efficiency of P2H
- H_c The higher heating value of hydrogen
- π^g, π^e, π^h Ratio of GV/EV/HV traffic demand
- $\delta_{a,\rho,rs}^g$ If path $\rho \in \lambda_g^{rs}$ passes link $a \in T_A^{rg}$, $\delta_{a,\rho,rs}^g = 1$; otherwise, $\delta_{a,\rho,rs}^g = 0$.
- $\delta_{a,\rho,rs}^e$ If path $\rho \in \lambda_e^{rs}$ passes link $a \in T_A^{ch}$, $\delta_{a,\rho,rs}^e = 1$; otherwise, $\delta_{a,\rho,rs}^e = 0$.
- $\delta_{a,\rho,rs}^h$ If path $\rho \in \lambda_h^{rs}$ passes link $a \in T_A^{ch}$, $\delta_{a,\rho,rs}^h = 1$; otherwise, $\delta_{a,\rho,rs}^h = 0$.
- t_a^0 Free flow travel time on link $a \in T_A^{rg}$
- c_a^{rg} Traffic flow capacity of link $a \in T_A^{rg}$
- $c_a^{ch,e}, c_a^{ch,h}$ Maximum allowable vehicular flow of charging link $a \in T_A^{ch}$
- $P_{ser,e}, P_{ser,h}$ Average service rate at charging stations
- E^e, E^h Charging demand of unit traffic flow.
- $t_{a, ch, e}^{max}, t_{a, ch, h}^{max}$ Maximum waiting time at charging stations
- $q_{rs,t}$ Trip rate (traffic demand) between O-D pair r-s
- ω Monetary cost of travel time.
- $\lambda_{a,t}^e, \lambda_{a,t}^h$ Charging price at charging stations
- $\mu_{e,t}$ Time of use price
- $\mu_{g,t}$ Unit price of natural gas
- N_{peak}, N_{valley} Number of peak and valley periods